Microfluidic Delivery of High Viscosity Liquids Using Piezoelectric Micropumps for Subcutaneous Drug Infusion Applications

Nivedha Surendran, Claudia Patricia Durasiewicz, Thalia Hoffmann, Axel Wille, Agnes Beate Bussmann, and Martin Richter

Abstract*—*Goal: **Auto-injectors for self-administration of drugs are usually refrigerated. If not warmed up prior to the injection, ejection of the total drug volume is not guaranteed, as their spring and plunger mechanism cannot adjust for a change in viscosity of the drug. Here, we develop piezoelectric micro diaphragm pump that allows these modifications possible while investigating the effectiveness of this alternative dosing method. *Methods:* The dosing of highly viscous liquid of 25 mPa·s is made possible using application-specific micropump design. By comparing the analytical with experimental results, the practicality of the concept is verified. *Results:* Using a powerful piezoelectric stack actuator, the micropump achieves high fluid pressures of up to (368 $\pm$ 17) kPa. In order to assess the influence of viscosity, we characterize the fluidic performance of the designed micropump through 27G gauge needle for various water-glycerin mixtures. We find maximum flow rates of 2 mL/min for viscosities of up to 25 mPa·s. *Conclusions:* The developed micro diaphragm pump enables the development of smart auto-injectors with flow rate regulation to achieve drug delivery for high viscosity drugs through 27G needles.**

***Index Terms*—27G needle, auto-injectors, high viscous mixtures, micropumps, piezoelectric stack actuator.**

***Impact Statement*—This research demonstrates that metal micropumps are capable of dosing highly viscous mixtures and thus provide an alternate approach with the possibility of further advancement for auto-injector applications.**

Manuscript received 24 July 2023; revised 13 November 2023 and 15 January 2024; accepted 15 January 2024. Date of publication 18 January 2024; date of current version 23 February 2024. This work was supported in part by the Moore4Medical project, which has received funding from the Electronic Components and Systems for European Leadership Joint Undertaking (ECSEL JU) in collaboration with the European Union's H2020 Framework Program under Grant H2020/2014–2020, and in part by the National Authorities, under Grant H2020-ECSEL-2019-IA-876190 www.moore4medical.eu. The review of this article was arranged by Editor Carlotta Guiducci. *(Corresponding author: Nivedha Surendran.)*

Nivedha Surendran, Thalia Hoffmann, Axel Wille, Agnes Beate Bussmann, and Martin Richter are with the Fraunhofer EMFT Institute for Electronic Microsystems and Solid-State Technologies, 80686 Munich, Germany (e-mail: nivedha.surendran@emft.fraunhofer.de; thalia.hoffmann@emft.fraunhofer.de; axel.wille@emft.fraunhofer.de; agnes.bussmann@emft.fraunhofer.de; martin.richter@emft.fraunhofer.de).

Claudia Patricia Durasiewicz is with the Fraunhofer EMFT Institute for Electronic Microsystems and Solid-State Technologies, 80686 Munich, Germany, and also with the Fraunhofer IMTE Research Institute for Individualized and Cell-based Medical Engineering, 23562 Lübeck, Germany (e-mail: claudia.durasiewicz@googlemail.com).

Digital Object Identifier 10.1109/OJEMB.2024.3355692

I. Introduction

TODAY, there is a rising prevalence of chronic illnesses, such as multiple sclerosis, rheumatoid arthritis, diabetes, and growth hormone insufficiency. All of the above illnesses necessitate the daily intake of drugs, often multiple times per day [1], [2]. In many cases, oral intake of drugs is infeasible due to low absorption or breakdown of the drug molecules in the digestive tract [3].

Hence, patients primarily self-administer medication by intravenous or subcutaneous injection.

State-of-the-art auto-injectors employ spring and plunger mechanisms and deliver medication in less than 15 seconds [1]. Many drug formulations are stored between 2 to 8°C, and are warmed up to ambient temperature prior to use [4], [5]. An insufficiently warmed auto-injector can lead to poor accuracy of the delivered volume, due to the formulation's higher viscosity [6], [7], [8]. As a result, the device fails to eject the complete drug volume, as the nominal force of the spring mechanism is fixed [9], [10]. A possible solution is an increased spring force to eject the fluid out of the injector [11], however, this approach increases the risk of uncontrolled fracture of a glass based drug reservoir [12], [13]. Despite recent improvements in reservoir and needle design, the risk still exists with spring powered autoinjectors. To ensure safe and accurate delivery in a large temperature range, an electronic auto-injector that adapts to changing viscosities is necessary. In our research, we provide an alternative approach to the frequently reported auto-injector failure state, such as incorrect dosage, by employing a micropump for drug dosing [14]. In future, by combining it with a temperature sensor, a micropump can be controlled to deliver the desired drug volume with respect to viscosity and therefore create a smart auto-injector system for reliable and precise drug dosing. To work towards such a smart system, we develop a micro diaphragm pump with a piezoelectric stack actuator capable of delivering fluids of a broad range of viscosity along with extended priming abilities.

There are many examples of micropump research for drug delivery applications with numerous alternative actuation methods [15]. Piezoelectric actuation is one of the most common types

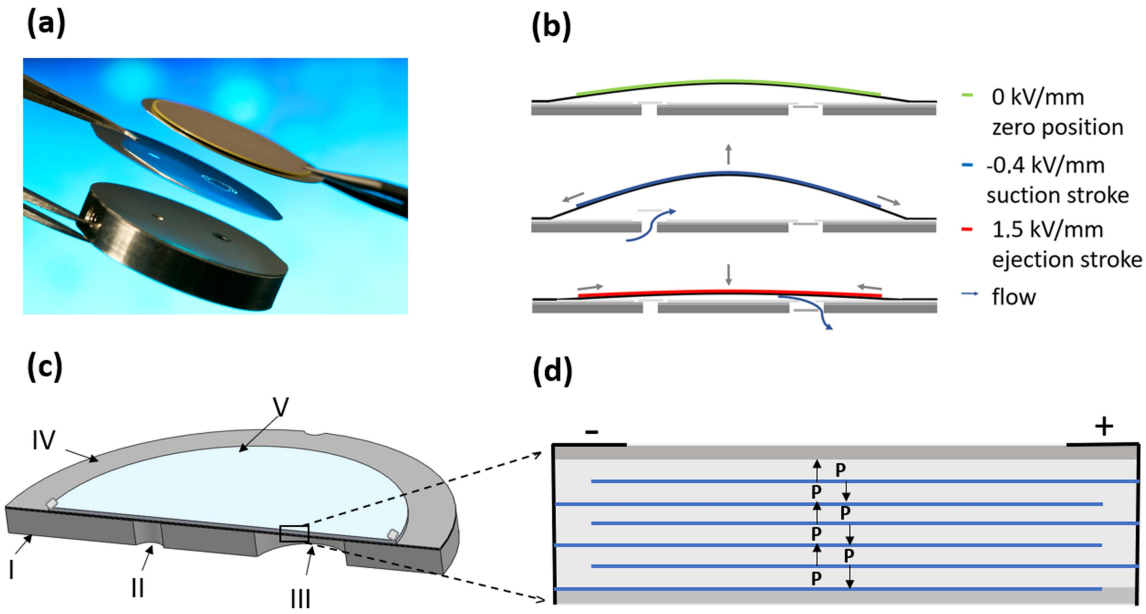

Fig. 1. (a) Parts of a piezoelectric metal micropump © Bernd Müller/Fraunhofer EMFT. (b) Working principle (adapted from [16]). (c) Cross sectional view of a pump denoting pump body (I), inlet (II) and outlet valves (III), piezoelectric actuator (IV) and glued actuator foil (V). (d) Cross sectional view of a multilayer piezoelectric structure with different directions of polarization.

as it delivers large flow rates and pressure, is simple to use, is energy efficient and is precise in operation. However, high actuation voltages of up to several hundred volts are frequently needed for piezoelectric actuation [15], [16]. Especially for high-pressure applications with thick actuators, voltages are high to generate the necessary electric field and, thus, elongation. Furthermore, the actuation signal is often asymmetrical, since high negative voltages cause depolarization of the actuator [17]. As a consequence, the required driving electronics are complex, costly, and large. Reducing the required actuation voltage is hence an aim of the research on piezoelectric micropumps [15]. One possibility to reduce the actuation voltage is the use of piezoelectric stack actuators at a lower driving frequency while maintaining sufficient flow rate [15]. Such actuators typically have a lower operational voltage. Especially for high pressure actuation, where large forces are required, the use of a bulk actuator require extreme voltages. The use of stack actuators allows to limit this voltage to 200 V.

Another crucial aim of development is to limit the patient's pain perception, which depends on the formulation's viscosity, injection volume, flow rate, and subcutaneous backpressure [9]. Subcutaneous backpressure is one of the most common causes for pain after injection [8]. It depends on the injection flow rate and rises for higher flow rates [18]. A typical auto-injector produces a mean pressure of (24 $\pm$ 3.4) kPa when injecting 6 mL/min and (7.8 $\pm$ 7.8) kPa while injecting 1 mL/min [18]. In addition, it is found that the subcutaneous tissue can tolerate large-volume injections with little backpressure as long as flow rates are as low as $\leq$2 mL/min [18]. Generally, injecting a viscous mixture of 15–20 mPa·s at a 1.2 mL/min flow rate is likely to be well accepted without causing pain [18]. Thus, this research aims to develop a micropump capable of delivering a minimum of 1 mL/min of flow rate for high-viscosity liquids for the envisaged auto-injector application. The micropump shall achieve this flow rate while delivering the liquid through a 27G needle, creating an additional flow resistance as it would be the case in the pen-injector application. The micropump shall also deliver precise doses adjusted to the viscosity of the drug, while the pump design shall be small to allow integration into a hand-held auto-injector device.

II. Materials and Methods

The goal of this study is to design, manufacture, and test a high flow rate micropump to dose highly viscous mixtures. The fabrication process, theoretical modelling as well as experimental evaluations are described in this section.

The piezoelectric micro diaphragm pump developed for this study is based on the work presented by Bußmann, Durasiewicz et al. [16], who give a detailed description of the manufacturing process. A total of 8 samples are manufactured. Each sample consists of a steel body and glued on piezoelectric disk actuator. Fig. 1(a) depicts different parts of a stainless-steel pump: A base plate, two valve foils, and an actuator foil. The pump is piezoelectrically actuated as shown in Fig. 1(b). An alternating voltage causes the diaphragm to oscillate and thus leads to a volume displacement. The two passive spring valves rectify this fluid movement, leading to an effective flow. To enable pump design with a very high compression ratio [19], we follow a specific pretension technique introduced by Herz et al. [20] during the fabrication process.

A. Analytical Modeling of a Piezoelectric Micropump for High Viscous Liquids

In general, injecting high viscosity drugs through needles with a small diameter can cause injectability issues [21]. Enlarging

the needle bore size decreases the fluidic resistance of the setup, and consequently less pumping pressure is required. While this simplifies the whole injection process, a larger bore size increases the patient's perceived pain [22], [23]. To minimize patient discomfort, a narrow needle must be used, which requires a sufficient pumping pressure. Hence, the achieved pressure of the pump is the main optimizing parameter in designing an effective micropump mechanism. The resulting flow rate of the pump will depend on the geometry and mechanical properties of the pump, piezoelectric actuator, the properties of the transported fluid, as well as potential disturbances such as occurrence of bubbles. The analytical model described in the following section, elaborates the dependence of the flow rate on these parameters.

1) Modeling of the Piezoelectric Stack Actuator: The circular plate monomorph piezoelectric actuator is described in detail by Herz et al. [24], [25] as a linear model considering the following parameters: volume displacement depending on the pressure difference $p - p_0$ (with pump chamber pressure p and atmosphere pressure p_0), the applied voltage $U - U_0$ (with ground voltage U_0), the fluidic capacitance of the piezoelectric bending actuator C_M, and the volume coupling factor of the piezoelectric bending actuator $C_E{}^*$. The coefficients C_M and $C_E{}^*$ depend on the radii of the piezoelectric ceramic R_p and diaphragm R_d, the thicknesses of the piezoelectric ceramic T_P and diaphragm T_d, the Young's moduli of the piezoelectric ceramic Y_p and diaphragm Y_d, and the Poisson ratio ν of the diaphragm. Equation (1) provides the corresponding expression.

$$V\,(p,U) = C_M\,(p - p_0) + C_E^*\,(U - U_0) \tag{1}$$

The maximum stroke volume ΔV (without back pressure) of the micropump is defined as the volume displaced with a single actuator movement while applying voltage levels of U_+ and U_- at atmospheric pressure p_0:

$$\Delta V = -C_E^*\,(U_+ - U_-) \tag{2}$$

Furthermore, the volume coupling factor $C_E{}^*$ is proportional to the transversal piezoelectric coefficient d_{31}. Generally, a piezoelectric stack actuator has N active layers (with an overall thickness of $T_{\text{active}} = N \times T_{\text{layer}}$) covered by two inactive isolation layers at the top and bottom (with a thickness of T_{inactive}). The fluidic capacitance C_M) is calculated using the entire thickness of the piezo ceramic, $T_p = T_{\text{active}} + T_{\text{inactive}}$ (all active layers and both inactive layers), as all layers contribute to the mechanical stiffness of the ceramic. Contrarily, we consider only the active layers for calculation of the volume coupling factor $C_E{}^*$). The analytical expressions required to calculate C_M and $C_E{}^*$ are given by Herz et al. [25].

2) Estimation of the Maximum Flow Rate: We estimate the maximum flow rate $Q_{\max}$ with a simplified model [26], where the pressure increase is defined by the voltage rise time, whereas the pressure decay is exponential and defined by the typical stroke time τ_{stroke}. This can be considered as the time to move the stroke volume ΔV in and out of the pump chamber. It can be further described as the product of the fluidic capacitances (C_M of the diaphragm and C_{gas} of a potential gas bubble in the pump chamber) and the fluidic resistances of the laminar friction at the valve R_{valve} and at the pump chamber R_{chamber}:

$$\tau_{\text{stroke}} = (R_{\text{valve}} + R_{\text{chamber}})\,(C_M + C_{\text{gas}}) \tag{3}$$

Following the exponential decrease of the pressure (as described in [26]), only about 63% of the entire stroke time τ_{stroke} is performed, after $3 \times \tau_{\text{stroke}}$ this value is about 95%. Thus, we approximate the maximum pump flow rate $Q_{\max}$ by taking a time of $3 \times \tau_{stroke}$ for the suction mode to suck the fluid into the pump chamber. Similarly, fluid ejection mode to eject the fluid out of the pump chamber also requires the same time. Therefore,

$$Q_{\max} \approx \frac{\Delta V}{6\tau_{stroke}} = \frac{\Delta V}{6\,(R_{valve} + R_{\text{chamber}})\,(C_M + C_{\text{gas}})} \tag{4}$$

To optimize $Q_{\max}$, a large stroke volume and small flow resistances at the valve and in the pump chamber are required. The above-mentioned flow resistances are modeled by considering the pump geometry as shown in Fig. 2.

When highly viscous fluids flow through narrow gaps such as the valve seat Q_V and the pump chamber Q_{pk} or the needle capillary Q_{cap}, the Reynolds numbers are small. Therefore, the generated laminar friction is the dominant effect that limits the flow rate.

For a laminar flow of an incompressible, Newtonian fluid we approximate the flow through the pump chamber Q_{pk} with the law of Hagen Poiseuille, assuming a square cross section of the flow path (as Fig. 2):

$$Q_{pk} = \frac{b_{pk}\,h_{pk}^3}{12\,\eta\,l_{pk}}\Delta p_{pk} = \frac{1}{R_{\text{chamber}}}\Delta p_v \tag{5}$$

The flow Q_V through restriction at the valve seat is given by the laminar, radial gap flow of a round plate valve [27]:

$$Q_v = \frac{\pi\,h_v^3}{6\,\eta\,ln\,\frac{r_1}{r_0}}\Delta p_v = \frac{1}{R_{\text{valve}}}\Delta p_v \tag{6}$$

All the above-described parameters are depicted in Fig. 2. Both the height of the valve gap h_V and the height of the pump chamber h_{pk} are not constant, but vary during the pump cycle. Thus, we consider the worst-case scenario for the height of the diaphragm h_{pk} when the diaphragm is at the lower turning point (at maximum positive voltage). The reason for that is due to the third power of h_{pk} in (5), the flow resistance at this lower turning point contributes much more to the flow resistance compared to the upper turning point.

Similarly, the flow characteristics at the valve region are also not linear. The resistance is very high for small valve openings (at the end of the suction and the ejection mode, where we have small pressure differences at the valves) and low resistance at large valve openings (at the beginning of the suction and the ejection). Therefore, we use an effective pressure to calculate a mean valve opening h_v heuristically. This effective pressure is small compared to the actuator's blocking pressure p_{block} which is the maximum backpressure that a micropump can achieve. We calculate the opening h_V at the maximal gas back pressure $p_{\max,\text{gas}}$ that is mainly defined by the compression ratio, to estimate the influence at the flow restriction of the valve to the maximum flow rate $Q_{\max}$.

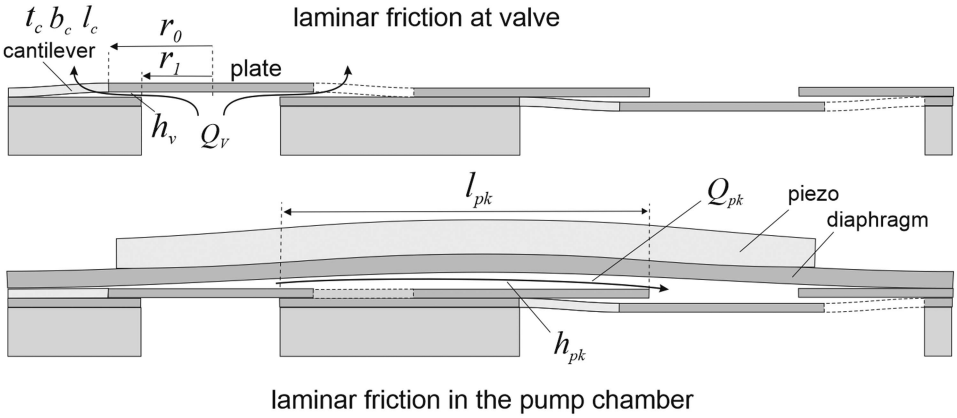

Fig. 2. Gap geometry at the valve and in the pump chamber defining the flow resistances: both gaps have a height varies during the pump cycle due to valve movement and actuator diaphragm movement.

Optimization goals to design a micropump for the delivery of highly viscous fluids are derived from the previous equations: Firstly, the length of the valve gap has to be minimized ($l_{valve} = r_0 - r_1$). This length is limited by fabrication tolerances, such as etching precision of the foils, and alignment precision during laser welding. Secondly, the length of the pump chamber l_{pk} has to be reduced by arranging the fluidic ports as closely to the center as possible. Lastly, the height of the pump chamber h_{pk} can be adjusted by increasing the pretension of the piezoelectric diaphragm actuator [16], [28] as well as the voltage levels of pump operation. In this study, we select a pretension field of 1.5 kV/mm to increase the pump chamber height. However, there has to be a trade-off with other design parameters like compression ratio, as higher pretension reduces the compression ratio and thus reduces the bubble tolerance.

3) Reduction of the Flow Rate by Laminar Friction in the Needle and Body Pressure: The effective pump flow rate through the needle Q_p decreases linearly with back pressure p_p

$$Q_p = Q_{\max}\left(1 - \frac{p_p}{p_{\text{block}}}\right) \tag{7}$$

While the blocking pressure p_{block} is expressed by [24]:

$$p_{\text{block}} = -\frac{C_E^*}{C_M}\left(U_+ - U_-\right) = \frac{\Delta V}{C_M} \tag{8}$$

In addition to the body pressure of the patient p_{body}, the pressure loss at the 27G needle must be considered. The pressure loss at this capillary p_{cap} with the cross-section A and the length L is given by the law of Hagen Poiseuille:

$$p_{\text{cap}} = R_{\text{cap}} Q_p = \frac{8\pi\eta L}{A^2} Q_p \tag{9}$$

The total required delivery pressure p_p consists of p_{cap} and the body pressure p_{body}

$$p_p = p_{\text{cap}} + p_{\text{body}} \tag{10}$$

Combining (8), (9), and (10) gives an expression of the flow rate Q_p through the needle (capillary) into the body of the patient:

$$Q_p = Q_{\max}\frac{1 - \frac{p_{\text{body}}}{p_{\text{block}}}}{1 + \frac{Q_{\max} R_{\text{cap}}}{p_{\text{block}}}} \tag{11}$$

To maximize the achieved flow rate through the needle during subcutaneous injection, a large blocking pressures p_{block} is required in addition to the large maximal flow $Q_{\max}$ and a small body pressure p_{body}. So,

$$p_{\text{block}} \gg p_{\text{body}} \tag{12}$$

$$p_{\text{block}} \gg Q_{\max} R_{\text{cap}} \tag{13}$$

However, with a high viscosity, the resistance of the needle capillary R_{cap} gets large. To realize very large blocking pressures at reasonable voltage levels, a stack actuator is chosen.

Inserting (2), (4), and (8) into (11), we get a comprehensive analytical model to roughly estimate the achievable flow rate Q_p of viscous liquids by a micropump through a needle by the following expression:

$$Q_p = \frac{p_{\text{block}} - p_{\text{body}}}{6\left(R_{valve} + R_{\text{chamber}}\right)\frac{(C_M + C_{\text{gas}})}{C_M} + R_{\text{cap}}} \tag{14}$$

Along with the other parameters,

$$R_{\text{valve}} = \frac{6\,\eta\, ln\,\frac{r_1}{r_0}}{\pi\, h_v^3} \tag{15}$$

$$R_{\text{chamber}} = \frac{12\,\eta\, l_{pk}}{b_{pk}\, h_{pk}^3} \tag{16}$$

$$R_{\text{cap}} = \frac{8\pi\eta L}{A^2} \tag{17}$$

$$p_{\text{block}} = -\frac{C_E^*}{C_M}\left(U_+ - U_-\right) = \frac{\Delta V}{C_M} \tag{18}$$

Where,

η: viscosity of the liquid

U_+ and U_-: positive and negative voltage levels

p_{body}: body pressure at the injection location (which depends on Q_p)

p_{block}: blocking pressure of the micropump, considering the actuator geometry (such as the diameter and thicknesses of piezo ceramic and diaphragm), the d_{31} coefficient of the piezo ceramic, the young moduli of piezo ceramic and diaphragm, as well as the Poisson number and the voltage levels

C_M: fluidic capacitance of the actuation diaphragm, considering the actuator geometry, the young moduli of piezo ceramic and diaphragm as well as Poisson number

C_E^*: volume coupling factor of the piezo/diaphragm actuator, which depends on the same parameter like C_M, and is additionally proportional to the transversal piezo ceramic coefficient d_{31}.

C_{gas}: fluidic capacitance of a (potential) air bubble in the pump chamber with the Volume V_{gas}, considering the volume of the gas bubble. In the worst case, the volume of the gas bubble corresponds to the entire dead volume of the pump chamber [31].

r_1, r_0: geometry parameter of the valve plate (as seen in Fig. 2)

h_{pk}: height of the pump chamber, if the actuator is at the lowest position at positive voltage, considering the pretension and the voltage levels

l_{pk}: length of the pump chamber between both valve cavities

b_{pk}: width of the pump chamber

h_v: opening of the valve at the maximum pressure, which the pump can achieve with gases

L, A: length and the diameter of the needle

Thus, to maximize the flow rate Q_p, the following measures have been realized in the development process:

- Blocking pressure is increased by increasing the thickness of the piezoelectric actuator Tp , diaphragm Td, driving the piezo ceramic with a high electrical field (E+ = U+/ Tlayer and E- = U-/ Tlayer), and using a piezo ceramic material with a high d31 coefficient.
- Reduce the resistance of the pump chamber according to (5), by increasing hpk (by a higher pretension and adjusted voltage levels), and
- Reduce the resistance of the valve according to (6), by reducing the gap length r1-r0.

B. The Impact of Gas Bubbles as a Disturbance of Micropumps Pumping High Viscous Liquids

Since the maximum flow rate Q_{max} (4) as well as the flow rate through the needle Q_p (14) depends on the fluidic capacitances, gas bubbles are a significant disturbance. If a large bubble with a volume V_{gas} enters the pump chamber, the fluidic capacitance $(C_M + C_{gas})$ increases by a significant factor, reducing Q_{max} and consequently Q_p. One common strategy to reduce the impact of gas bubbles is to minimize the dead volume V_0 of the pump chamber, as the volume of the gas bubble cannot exceed the dead volume V_0 and with that increasing the compression ratio $\Delta V/V_0$.

However, a significant reduction of the dead volume V_0 requires the reduction of the pump chamber height h_{pk}, which is increasing the flow resistance, as per (5).

Furthermore, this situation is complicated by (8) where a high blocking pressure p_{block} is associated with a small fluidic capacitance C_M, with that the fluidic capacitance C_{gas} of even small bubbles are dominating the term $(C_M + C_{gas})$ in (14).

Next, to increase the compression ratio $\Delta V/V_0$ to increase the pump's robustness against bubbles, the stroke volume ΔV must be increased. A large stroke volume contradicts to a high blocking pressure p_{block}.

In fact, it is not possible to create a micropump that is able to pump both highly viscous liquids and maintain the same stroke volume if a bubble is entering the micropump. Bubbles in the pump chamber are always a significant disturbance for high-viscosity drug dosing micropumps, which are reducing Q_p according to (14). Our strategy is to create a pump with a compression ratio that is high enough to be bubble-tolerant and to transport the bubble (with a momentary smaller flow rate, according to (14)) through the pump chamber and return to Q_p when the gas bubble is ejected out of the pump.

Thus, in accordance with the model aforementioned, a stiffer piezoelectric stack actuator with 13 electroactive layers is chosen to meet the requirement of a minimum 1 mL/min flow rate at 25 mPa·s. The piezoelectric actuator has a diameter of (16 ± 0.3) mm vertically and (14 ± 0.3) mm horizontally and is bonded to a steel actuator foil of 200 μm. The individual piezoelectric actuator has a total thickness of (0.68 ± 0.15) mm, of which each active layer is $T_{active} = 40$ μm thick and the non-active/isolation layer is 16 μm thick. The use of a 13 layer stack actuator allows to limit the actuation voltage to 130 $V_{peak\text{-}to\text{-}peak}$. To achieve similar fluidic performance with a bulk actuator of comparable active layer thickness would require about 1000 $V_{peak\text{-}to\text{-}peak}$. For experimental evaluations, a total of 8 pump samples are manufactured and obtained results are discussed in the following sections.

C. Actuator Stroke Measurements

The actuator deflection directly correlates to the volume of fluid displaced within one stroke and is, thus, an important measure for pump quality. Therefore, the actuator stroke height is an important performance metric of a micropump and determined in static deflection analysis.

The actuators are characterized by applying a quasi-static voltage for a fixed time of ~2s without an influence of liquid medium (Voltage amplifier SVR 5003, piezo system Jena GmbH) while measuring their deflection optically with the white light interferometric profilometer (Fries Research and Technology) exactly at the center of the piezo ceramic where the deflection is maximal under excitation. The optical sensor used has a range of 3 mm and a maximal resolution of 30 *nm*. The applied electric field to measure the hysteresis of the piezo ceramic actuator is −0.38 to 2.9 kV/mm. The measurement accuracy of the total actuator stroke is known to be 2 μm, which was evaluated from the repetitive measurements of several

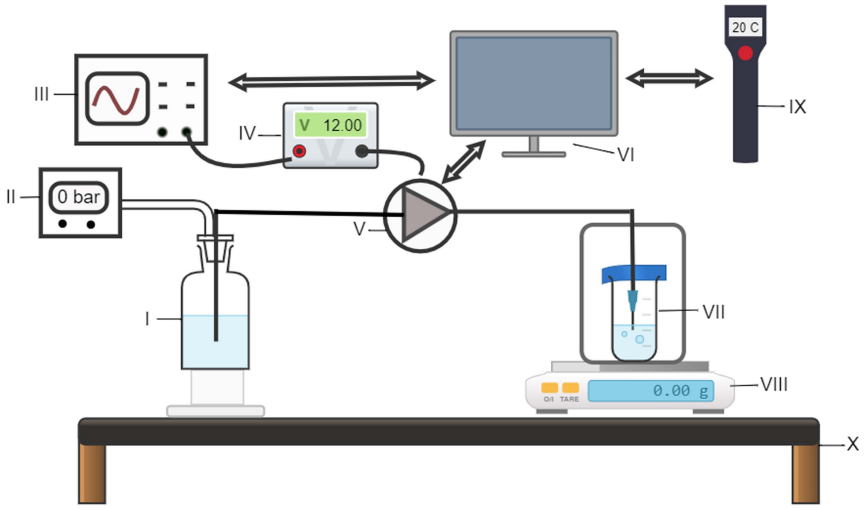

Fig. 3. Gravimetric test setup. Inlet (I), Pressure Controller (II), Waveform generator (III), Amplifier (IV) Micropump (V), Data processor (VI) Taped outlet reservoir placed on the scale (VII) Weighing scale (VIII); Ambient Temperature sensor (IX); Vibration isolated test bench (X).

samples [16]. The results of this assessment are discussed in the upcoming section. Furthermore, the achievable actuator stroke directly correlates to the elongation of the piezoelectric disc actuator. Therefore, the direct measurement of the piezoelectric elongation curve of the stack actuator helps us to gain a better understanding of the chosen actuators for the new pump design. Therefore, we also evaluate the field dependent elongation using the white light interferometric profilometer by incorporating the experimental setup described by Bußmann et al. [28].

D. Fluidic Measurements

The manufactured micropump samples are fluidically characterized with DI water at room temperature. As an initial measurement, the frequency dependent flow rate is evaluated for sinusoidal actuation excited at the voltage amplitude of $-15\ V$ to $115\ V$ (-0.38 to 2.9 kV/mm) for 0–60 Hz. Later, the pressure-dependent flow rate behavior is also evaluated by actuating the pumps with a constant 30 Hz sinusoidal actuation up to a backpressure of 150 kPa. Finally, the passive backwards leakage rate is measured by applying a small backpressure of up to 5 kPa, while the pump is not actuated.

The sensors used for all the above-mentioned measurements are Coriolis flow sensors (Bronkhorst mini cori-flow M14: range 0.5 mL/min to 167 mL/min, accuracy: $\pm 0.2\%$), Pressure controller (Mensor CPC3000: range -50 kPa to 200 kPa, accuracy: ± 0.05 kPa) and Keysight 33500B Waveform generator along with high voltage amplifier SVR 1000/3 channel (Voltage range: $-200\ V$ to $+1000$ V from piezosystem Jena).

E. Gravimetric Flow Rate Characterization

The use of the above mentioned Coriflow sensors is limited to DI water. Hence, the flow characterization for liquids of different viscosities is conducted with a gravimetric setup. Despite the possibilities of optical flow monitoring and photometric methods, most investigations rely on gravimetric measurements as they are well suited for all types of testing liquid [30]. A schematic representation of the experimental gravimetric test station is shown in Fig. 3.

We conduct our gravimetric measurements with a high-precision microbalance 225S from Sartorius. The outlet reservoir is placed on the weighing scale and filled with approximately 20 mL of the same testing liquid that is delivered by the micropump. The outlet reservoir is covered with the Nitto Semiconductor Wafer Tape SWT 10+R to limit evaporation. The micropump is positioned in between the weighing cage and the inlet reservoir and connected by Tygon S3^{TM} E-3603 flexible, long-lasting and crack-resistant tubing with a length of 0.76 m. The end of the tube is fitted with a 27G gauge B.Braun sterican needle. These needles are widely used for subcutaneous, intramuscular, intravenous, and intra-arterial injections. Their dimensions are 20 mm in length and 0.4 mm in outer diameter. The inner diameter of the 27G needle is assumed to be 210 μm, which is an important parameter regarding the flow resistance of the needle [31]. The inlet and the outlet reservoirs are filled with the testing liquid such that their surfaces are leveled to prevent hydrostatic pressure differences. The balance as well as the micropump are placed on a vibration-free isolated granite table to reduce external mechanical vibrations. Additionally, the windshield cover from the microbalance isolates it from surrounding air convection. All measurements are conducted with the same experimental setup, as any change in the periphery could cause a considerable change in results. In order to represent high viscosity drugs, different Glycerol-water mixtures ranging from 2 mPa·s to 25 mPa·s are prepared at room temperature. Subsequently, we measure the dynamic viscosities of the prepared with a Sinewave SV-10 series Viscometer (range: 0.3 to 10000 mPa·s; repeatability of 1%).

F. Actuation Methodology

Experiments with viscous mixtures are conducted by actuating pumps at different electrical waveforms and different voltage amplitudes as shown in Table I. This varies the total actuator

TABLE I
ACTUATION METHODS USED FOR PUMPING OF HIGH VISCOSITY MIXTURES

Actuation method	Applied waveforms	Excitation Voltage/Electric Field (*V* or *kV/mm*)
Standard	Sinusoidal and Rectangular	15 to 115 *V* or -0.38 to 2.9 *kV/mm*
Voltage amplitude expansion	Sinusoidal and Rectangular	-45 to 115 *V* or -1.13 to 2.9 *kV/mm*
Voltage offset variation	Sinusoidal	-30 to 100 V or -0.75 to 2.5 *kV/mm*

movement, average chamber height and achieved maximum pressure in the pump chamber.

In sinusoidal actuation, the applied voltage varies gradually according to the sine function. Consequently, the actuator deflection happens transiently. Due to gradual pressure build-up, passive spring valves open and close transiently, potentially causing backflow through partially closed valves [16], and high frictional losses. On the contrary, when a rectangular actuation signal is applied, it results in rapid actuator movement, thereby causing large pressure peaks to build up inside the pump chamber. This ultimately results in rapid passive spring valve movement to their maximum opening position and thus, backflow is reduced and frictional losses at the valve are minimized. Therefore, the net flow rate can be increased by the rectangular actuation. However, a detrimental effect of rectangular actuation is the rapid deflection, which might exert exceedingly high mechanical stress on the piezo ceramic as well as on the dosed medium [16]. With this study, we intend to find the most effective and robust actuation signal for micropump operation.

Another factor that influences the total displacement volume is the applied voltage amplitude. By offsetting the voltage of the standard approach, the gap height between the actuator diaphragm and the bottom of the pump chamber is increased without compromising the total stroke volume. For lower viscosities, the dynamic friction coefficient is independent of the velocity of the medium, but for the highly viscous medium, the dynamic friction coefficient increases when the velocity increases [32]. Thus, this method is aimed at combating the frictional forces by decreasing the fluid's velocity and its proximity to the walls or the surrounded surface region.

The last variation introduced in this study is increasing the applied voltage amplitude. As the maximum flow rate $Q_{\max}$ directly depends on the total actuator stroke ΔV as per (4), in this technique, ΔV is increased by increasing the applied negative voltage during excitation. Results from previous studies support our approach, as they show that exciting the piezoelectric actuator at 30 to 40% of coercive field strength E_c can be pushed further up until 95% of E_c while stable operation is maintained up to 1 million cycles of repeated excitation [17], [33]. With the presented approaches, this study aims to choose an optimal electrical actuation method for different viscosities.

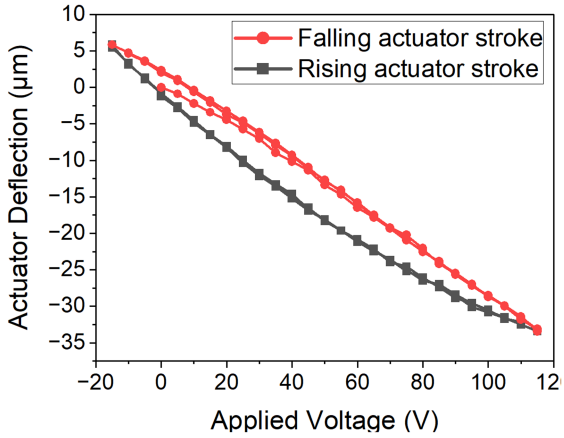

Fig. 4. Actuator stroke of an exemplary pump sample.

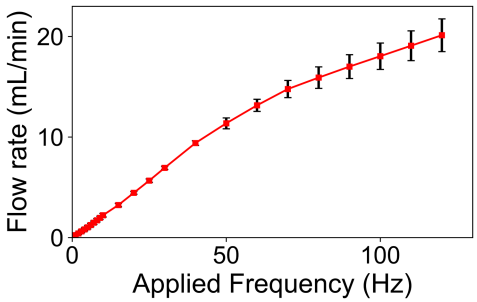

Fig. 5. Influence on the water-flow behavior of the micropump at −15/115 *V* sinusoidal actuation at operating frequencies from 0 to 120 Hz.

III. RESULTS AND DISCUSSION

For a better understanding of the stack actuator, it is experimentally analyzed before assembling the pump samples. The capacitance of the stack actuators is (782.3 ± 7.9) *nF*. The evaluation of the piezoelectric elongation of the overall three individual samples results in a large signal piezoelectric elongation coefficient of $d_{31} = 260 * 10^{-9}$ *C/N*. The elongation per applied field is therefore lower, compared to the previously used bulk actuator discs [28]. This is expected, since the stack actuator consists of a material with a lower d_{31} coefficient and includes additional passive layers as isolation.

Basic characterizations such as quasi-static stroke measurement and fluidic tests with DI water allow to evaluate the general properties of the new micropump design. The quasi-static stroke measurement results in the overall stroke height of the piezoelectric actuator of (39.97 ± 0.04) μm. Fig. 4 shows an exemplary stroke measurement. The total stroke height is the difference of the highest and the lowest position of the bending actuator and is obtained from the hysteresis curve. The total stroke height is an indication of stroke volume and determines the overall flow rate of the pump. The obtained actuator stroke is considerably lower than that of previous design of Fraunhofer EMFT micropumps – for instance, measured total actuator stroke for steel micropumps with bulk piezoelectric actuator of 200 μm thickness is (79.8 ± 2.9) μm [34]. This is due to the increased stiffness of this design.

Fig. 5 depicts the water flow behavior of the micropumps under sinusoidal actuation. In theory, the relationship between

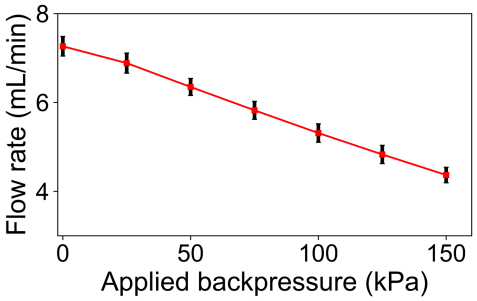

Fig. 6. Backpressure dependent flow rate with water at −15/115 *V* and 30 Hz sinusoidal actuation.

driving frequency (f) and flow rate (Q) is linearly proportional. As the driving frequency increases, maximum attainable flow rate also increases linearly until ($f_{cut-off}$). This region is called linear operation range. For higher frequencies, the flow rate increase follows a non- linear characteristic, reaches its maximum ($Q_{\max}$), and starts to decline. There are various reasons for declining flow rate with increased actuation frequency. In this case, the flow rate declines due to dynamic damping effects and inertial effects of the pump chamber, the check valves, and the fluidic periphery. Another effect can arise by driving the actuator close to its resonance frequency range, where a decline in flow rate is caused by vibration of the actuator [35], [36]. However, the latter effect is unlikely to affect the flow behavior of our micropumps, as the resonant frequency is in the *kHz* range [37].

The results show that the achieved flow increases steadily throughout the whole measured range up until 120 Hz. The maximum achieved water flow rate of the pumps at 120 Hz is (20.12 ± 1.52) mL/min.

In addition to operating frequency, the backpressure present in the system also influences the generated flow rate of the micropump. Fig. 6 shows the achieved flow rates in dependence of the applied backpressure. It is observed that the extrapolated blocking pressure obtained with DI water at 30 Hz sinusoidal actuation is (367.5 ± 16.7) kPa. In previous studies, the extrapolated blocking pressure achieved by our pumps with bulk piezoelectric actuator was approximately 75 kPa [16]. Thus, the described stack actuator design is capable of attaining higher blocking pressure at low operating voltages.

In addition to active flow characterization, the passive leakage rate is an important characteristic of micropumps. All the samples show a leakage rate of less than (0.03 ± 0.02) mL/min when small back pressure ranges of 0 to 5 kPa are applied. This value is well comparable to our previously presented pumps with an average leakage rate of (0.05 ± 0.04) mL/min [16]. This small leakage rate is a functional outcome of the passive spring valves, which are of the same design for all pump models [16], [34].

A. Performance Analysis With Viscous Medium

In order to evaluate the pump performance of our micropumps, we test their ability to deliver the minimum required flow rate of 1 mL/min. We conduct frequency sweep experiments for different viscous mixtures for the extended frequency range (0 to 120 Hz) to investigate the highest achievable flow rates and suitable operating range. The analytical and experimental

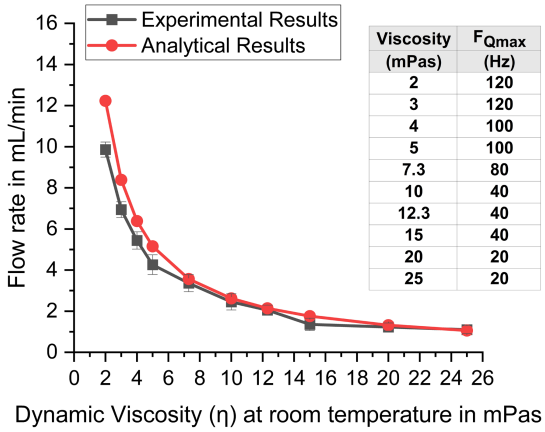

Viscosity (mPas)	F_{Qmax} (Hz)
2	120
3	120
4	100
5	100
7.3	80
10	40
12.3	40
15	40
20	20
25	20

Fig. 7. Maximum pump flow rate comparison between analytical and experimental results for standard sinusoidal actuation of −15/115 *V* for various viscous mixtures (η = 2 to 25 mPa·s) and corresponding operating frequency.

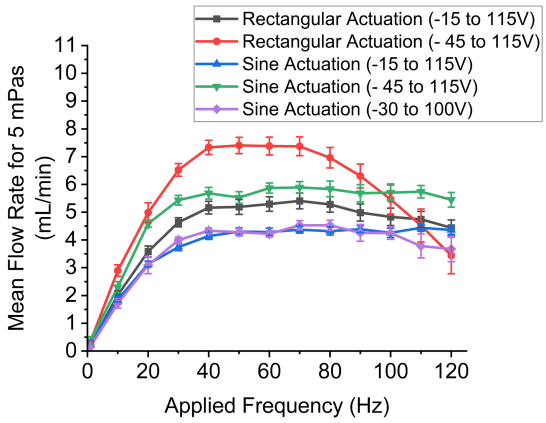

Fig. 8. Flow behavior comparison between rectangular and sinusoidal actuation at different voltage levels (−15 to 115 *V*), (−30 to 100 *V*) and (−45 to 115 *V*) for $\eta = 5$ *mPa·s*.

results are compared in Fig. 7 to show the obtained flow rates at various viscosities. We observe that, as the viscosity increases, the maximum attainable flow rate and the corresponding operating frequency decrease exponentially. This is because at higher viscosity, fluid damping and viscous effects dominate, and thus the maximal flow rate occurs at lower operating frequencies. At η = 25mPa·s, the micropump is able to deliver the required flow rate of 1 mL/min. Therefore, considering the potential auto-injector application, this actuator design yields a promising result by successfully establishing high viscous fluid transport. Comparing this experimental data with our analytical modeling, it is evident that the results are in good agreement.

To improve the generated flow rate even further, we investigate the effect of using different driving signal variants and voltage levels, as shown in Table II for 5 mPa·s and 25 mPa·s mixtures to represent medium and high viscosity liquids, respectively. The results are provided in Figs. 8 and 9. We observe that offsetting the applied voltage causes a similar flow behavior as the standard sinusoidal actuation in the linear range for a 5 mPa·s mixture. In contrast, when the same actuation is applied for 25 mPa·s, there is a remarkable improvement in the flow rate of around 1 mL/min (i.e., ≃99% increase in flow rate) at 10 Hz. However,

TABLE II
RESULTS OF MAXIMUM FLOW RATE OBTAINED UNDER VARIATION OF ACTUATION SIGNAL

Actuation method	Applied waveforms	Qp at 5 *mPa·s* at 50 *Hz*, in *mL/min*	Qp at 25 *mPa·s* at 20 *Hz*, in *mL/min*
Standard	Sinusoidal	4.30 ± 0.39	1.10 ± 0.18
Standard	Rectangular	5.18 ± 0.59	1.37 ± 0.35
Voltage offset variation	Sinusoidal	4.27 ± 0.32	2.19 ± 0.31 (10 *Hz*)
Voltage amplitude expansion	Sinusoidal	5.52 ± 0.56	1.88 ± 0.21
Voltage amplitude expansion	Rectangular	7.40 ± 0.65	2.67 ± 0.81

Sample sizes are N = 8 micropumps for sinusoidal, and N = 4 micropumps for rectangular actuation, respectively.

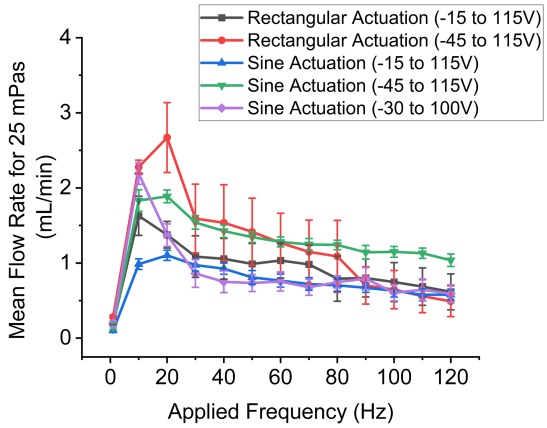

Fig. 9. Flow behavior comparison between rectangular and sinusoidal actuation at different voltage levels (−15 to 115 *V*), (−30 to 100 *V*) and (−45 to 115 *V*) for $\eta = 25$ *mPa·s*.

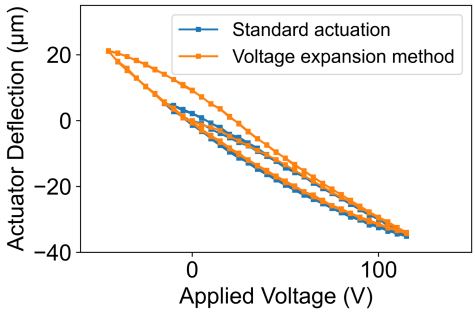

Fig. 10. Comparison between total stroke height for sinusoidal actuation at different voltage levels (−15 to 115 *V*) and (−30 to 100 *V*) corresponds to 40 μm and 54.1 μm, respectively.

at higher frequencies (the nonlinear range), we see an abrupt flow reduction.

One possible explanation for the improved flow behavior with rectangular actuation can be found in the valve opening time. While the actuator stroke is equal between sinusoidal and rectangular actuation, the acceleration of the fluid expelled out of the pump chamber is higher and the pressure rise time is shorter for the rectangular actuation. This pressure increase induces fast valves opening, such that high frictional losses in the valve gap during slow valve opening are mitigated. These differences in frictional losses become most evident at high viscosity.

In order to increase flow rate at low viscosities further, we analyze the impact of expanding the voltage amplitude for sinusoidal actuation. In this method, we aim for an increase of the total stroke volume by increasing the total stroke height, as shown in Fig. 10, which consequently increases the total stroke volume. This approach shows a substantial improvement in the flow rate for 5 mPa·s viscosity. This method results in a flow rate increase of 33.1% compared to the standard approach. Thus, increase in the stroke volume, show a greater improvement in the flow rate for moderately viscous fluids. At the same time, we observe a minor performance decrease when compared to the voltage offset variation approach for a 25 mPa·s viscous medium. In order to comprehend the resulting impacts, these intricate flow interactions need to be thoroughly studied using numerical and analytical modeling. However, the velocity gradient of the fluid and valve opening time can also explain this effect. The minimum gap height during a positive stroke increases the velocity of the fluid, thereby, producing high frictional effects. This could have resulted in a low flow rate.

Meanwhile for all the above-prescribed actuation approaches, a rectangular actuation yields a slightly higher flow rate for both medium and high viscosities. From a fluidic efficiency point of view, rectangular actuation improves the flow rate by creating fast actuator movement and building higher pressure peaks in the pump chamber. However, data from only 4 pump samples are used for data evaluations, as the total number of the 8 samples, 4 samples experienced functionality degradation. As pumps are subjected to rectangular waveform actuation, irreparable degradation of pump functionality occurs after pumping high viscosity fluid. Thus, the pumping efficiency is permanently degraded. But a complete electrical malfunction was not observed, as the capacitance measured on the piezoelectric actuator remained unchanged. The reason for this is during rectangular actuation, piezo ceramic expands and contracts instantaneously. This renders critical stress on the ceramic that in turn may induce some delamination of some of the electro-active layers in the stack actuator during operation. To eliminate foreign particles in the pump chamber as a possible root cause for pump degradation, the

micropumps were flushed with 70% isopropanol and 30% water mixtures and dried completely. However, pump functionality did not improve after a thorough cleaning. Thus, either electrical failure of the pumps, fatigue of the glue layer, or mechanical damage of the ceramics by microcracks are suspected as the true root cause of pump degradation. In the future, it is necessary to study the induced piezoceramic failure caused by rectangular actuation as well as possible mitigation approaches.

The presented results of our study lay the foundation for future integration of piezoelectric diaphragm pumps into commercial auto injectors. Even though comparable studies to build a higher-flow piezoelectric micropump to handle high backpressure have been published in the open literature [15], [38], [39], they are either large in size or have multiple pump chamber [40], [41]. Another recent interesting research claims that a miniaturized pump of size $11 \times 11 \times 1.5$ mm^3 produces a maximum water flow rate of 4.5 ml/min with an output pressure of 52 kPa driving at 50 Hz sinusoidal waveform with 180 $V_{peak\text{-}to\text{-}peak}$ [42]. However, as per the authors' knowledge, the influence of high viscosity and the needle on pump's performance has not yet been researched.

IV. Conclusion

In this study, a piezoelectric micro diaphragm pump with an adapted actuator design is presented for drug delivery application to enable adjustable flow rates for drugs with varied viscosity and temperature. For that, an analytical model is derived to estimate the maximum flow rate Q_p of the micropump through a thin 27G subcutaneous needle. This model considers the design of the piezoelectric actuator, the flow resistances of valve, pump chamber, and needle. Furthermore, the critical impact of a gas bubble to the flow rate Q_p is included in the analytical model. Through preliminary characterization with DI water without including gauge pressure, the system shows a flow rate of (20.12 $\pm$ 1.52) mL/min and a high backpressure capability of up to (367.5 $\pm$ 16.7) kPa. Later, a viscous medium and a 27G gauge needle are introduced to the system to evaluate the efficiency of the powerful stack actuator design. Various actuation signals, apart from standard sinusoidal actuation, are tested in order to find the most efficient and robust pump actuation. Above all, the voltage offset variation method under sinusoidal actuation yields a 2 mL/min flow rate for 25 mPa·s viscous mixtures. Later, expanding the applied voltage amplitude sinusoidal actuation to 0.9% E_c produces a higher flow rate for 5 mPa·s viscous mixtures. Meanwhile, for a rectangular actuation signal, higher flow rates are achieved but at the cost of electrical malfunction in the piezoelectric stack actuator. Hence, we improve the sinusoidal actuation method and are able to meet our minimum performance criteria. Our study is successful in providing insights into the intricate interactions of a micropumps with high viscous fluids and lays the foundation for further innovative developments in medical devices.

For future improvements of the current performance of the system the dynamic frictional losses need to be minimized. The main factors that contribute to these dynamic frictional losses are the moving passive spring valves and the deflecting actuator membrane. Therefore, adapting the geometry of the valve structure is a direct method to decrease frictional losses and maximize fluid transport. Additionally, an innovative needle design will improve the flow rate tremendously. Shorter needles with ultra-thin wall design not only increase the net outflow, but also prevent intramuscular injection risk and injection-related anxiety [43], [44]. In addition to designing a high-flow micropump, we would like to further evaluate the pump-medium interaction. Examples are the influence of a stiff microfluidic actuator on the stability of the drug or the impact of generated laminar friction on the change in the drug's temperature, which in turn induces a change in the viscosity of the drug.

Author's Contribution: Nivedha Surendran: Conceptualization, Data Curation, Formal Analysis, Investigation, Literature Resources, Visualization, Writing - Original Draft, Writing - Review and Editing.

Claudia Patricia Durasiewicz: Conceptualization, Methodology, Project Administration, Resources, Supervision, Validation, Writing - Original Draft, Writing - Review and Editing.

Thalia Hoffmann: Resources, Literature Resources.

Axel Wille: Funding Acquisition, Writing - Review and Editing.

Agnes Beate Bußmann: Project Administration, Supervision, Validation, Writing - Review and Editing.

Martin Richter: Methodology, Supervision, Validation, Writing - Original Draft, Writing - Review and Editing.

Conflicts of Interest:The authors declare no conflict of interest.

References

[1] A. V. Badkar, R. B. Gandhi, S. P. Davis, and M. J. LaBarre, "Subcutaneous delivery of high-dose/volume biologics: Current status and prospect for future advancements," *Drug Des., Develop. Ther.*, vol. 15, pp. 159–170, 2021, doi: 10.2147/DDDT.S287323.

[2] M. Zucker, "A review of reusable auto-injectors for biological & biosimilar drugs," *ONdrugDelivery Magazine*, Oct. 2017. Accessed: Mar. 17, 2023. [Online]. Available: https://www.ondrugdelivery.com/review-reusable-auto-injectors-biological-biosimilar-drugs/

[3] L. Bartz, C. Klein, A. Seifert, I. Herget, C. Ostgathe, and S. Stiel, "Subcutaneous administration of drugs in palliative care: Results of a systematic observational study," *J. Pain Symptom Manage.*, vol. 48, no. 4, pp. 540–547, 2014, doi: 10.1016/j.jpainsymman.2013.10.018.

[4] T. Laptoš and J. Omersel, "The importance of handling high-value biologicals: Physico-chemical instability and immunogenicity of monoclonal antibodies," *Exp. Therapeutic Med.*, vol. 15, no. 4, pp. 3161–3168, 2018, doi: 10.3892/etm.2018.5821.

[5] B. Kaufmann et al., "Heat-stability study of various insulin types in tropical temperature conditions: New insights towards improving diabetes care," *PLoS One*, vol. 16, no. 2, 2021, Art. no. e0245372, doi: 10.1371/journal.pone.0245372.

[6] T. Palm, "Temperature, viscosity, and concentration in parenteral drug development," 2015. Accessed: Oct. 27, 2022. [Online]. Available: https://bioprocessintl.com/manufacturing/monoclonal-antibodies/importance-concentration-temperature-viscosity-relationship-development-biologics/

[7] K. Monkos, "Viscosity analysis of the temperature dependence of the solution conformation of ovalbumin," *Biophysical Chem.*, vol. 85, no. 1, pp. 7–16, 2000, doi: 10.1016/S0301-4622(00)00127-7.

[8] A. Stelzl, "Subcutaneous delivery of high concentrated mAb-formulations using novel application systems," *J. Pharmaceut. Sci.*, vol. 111, no. 4, pp. 861–867, Apr. 2022.

[9] T. Thueer, L. Birkhaeuer, and D. Reilly, "Development of an advanced injection time model for an autoinjector," *Med. Devices: Evidence Res.*, vol. 11, pp. 215–224, 2018, doi: 10.2147/MDER.S151727.

[10] J. Cowperthwaite, "Auto-injector design: Managing drug temperature variations," *ONdrugDelivery Magazine*, May 2017. Accessed: May 23, 2022. [Online]. Available: https://www.ondrugdelivery.com/auto-injector-design-managing-drug-temperature-variations/

[11] M. Roe, "Challenges in high-viscosity, high-volume drug delivery," *ONdrugDelivery Magazine*, Oct. 2021. Accessed: Sep. 14, 2022. [Online]. Available: https://www.ondrugdelivery.com/challenges-in-high-viscosity-high-volume-drug-delivery/

[12] J. Philippson, "The interface between prefilled syringe and autoinjector – a development framework," *ONdrugDelivery Magazine*, Oct. 2019. Accessed: Jun. 9, 2023. [Online]. Available: https://ondrugdelivery.com/the-interface-between-prefilled-syringe-and-autoinjector-a-development-framework/

[13] F. DeGrazio and D. Paskiet, "Glass breakage, delamination and compatibility with biologics have boosted interest in novel materials in pharma packaging," The Free Library, 2012. Accessed: Jun. 9, 2023. [Online]. Available: https://www.contractpharma.com/issues/2012-01/view_features/the-glass-quandary/

[14] T. Weinhold, M. Del Zotto, J. Rochat, J. Schiro, S. Pelayo, and R. Marcilly, "Improving the safety of disposable auto-injection devices: A systematic review of use errors," *AAPS Open*, vol. 4, no. 1, pp. 1–14, 2018, doi: 10.1186/s41120-018-0027-z.

[15] A. B. Bußmann, L. M. Grünerbel, C. P. Durasiewicz, T. A. Thalhofer, A. Wille, and M. Richter, "Microdosing for drug delivery application—A review," *Sensors Actuators A: Phys.*, vol. 330, no. 6, 2021, Art. no. 112820, doi: 10.1016/j.sna.2021.112820.

[16] A. B. Bußmann, C. P. Durasiewicz, S. H. A. Kibler, and C. K. Wald, "Piezoelectric titanium based microfluidic pump and valves for implantable medical applications," *Sensors Actuators A: Phys.*, vol. 31, 2021, Art. no. 112649, doi: 10.1016/j.sna.2021.112649.

[17] A. Bußmann and L. Grünerbel, "Increasing piezo micro diaphragm pump performance by optimizing piezo actuation," in *Proc. IEEE Smart Syst. Integration; 13th Int. Conf. Exhib. Integration Issues Miniaturized Syst.*, 2019, pp. 1–4.

[18] D. V. Doughty, C. Z. Clawson, W. Lambert, and J. A. Subramony, "Understanding subcutaneous tissue pressure for engineering injection devices for large-volume protein delivery," *J. Pharmaceut. Sci.*, vol. 105, no. 7, pp. 2105–2113, 2016, doi: 10.1016/j.xphs.2016.04.009.

[19] P. Woias, "Micropumps - past, progress and future prospects," *Sensors Actuators B: Chem.*, vol. 105, no. 1, pp. 28–38, 2005, doi: 10.1016/j.snb.2004.02.033.

[20] M. Herz, M. Richter, and M. Wackerle, "Method for manufacturing a bending transducer, a micro pump and a micro valve, micro pump and micro valve," US Patent US9410641B2, Mar. 5, 2010.

[21] Q. Zhang, M. A. Fassihi, and R. Fassihi, "Delivery considerations of highly viscous polymeric fluids mimicking concentrated biopharmaceuticals: Assessment of injectability via measurement of total work done 'WT'," *AAPS PharmSciTech*, vol. 19, no. 4, pp. 1520–1528, 2018.

[22] N. Suresh, V. Koteeswaran, V. Natanasabapathy, K. Kasabwala, and D. Kowsky, "Needle gauge influences pain perception during intrapulpal anaesthesia - a randomized clinical trial," *Eur. Endodontic J.*, vol. 5, no. 3, pp. 191–198, 2020, doi: 10.14744/eej.2020.38358.

[23] H. S. Gill and M. R. Prausnitz, "Does needle size matter?," *J. Diabetes Sci. Technol.*, vol. 1, no. 5, pp. 725–729, 2007, doi: 10.1177/193229680700100517.

[24] M. Herz, D. Horsch, G. Wachutka, T. C. Lueth, and M. Richter, "Design of ideal circular bending actuators for high performance micropumps," *Sensors Actuators A: Phys.*, vol. 163, no. 1, pp. 231–239, 2010, doi: 10.1016/j.sna.2010.05.018.

[25] Markus Herz, "Optimierung der förderrate einer piezoelektrischen hochleistungs-mikropumpe," Ph.D. dissertation, Lehrstuhl für Mikrotechnik und Medizingerätetechnik, Technische Universität München, München, Germany, 2011.

[26] R. Zengerle, W. Geiger, M. Richter, H. Ulrich, S. Kluge, and A. Richter, "Application of micro diaphragm pumps in microfluid systems," *Mechatronics*, vol. 60, pp. 34–55, Jun. 2019.

[27] C. P. Durasiewicz, S. T. Güntner, P. K. Maier, W. Hölzl, and G. Schrag, "Piezoelectric normally open microvalve with multiple valve seat trenches for medical applications," *Appl. Sci.*, no. 11, 2021, Art. no. 9252, doi: 10.3390/app11199252.

[28] A. Bußmann, P. Korzer, and C. Wald, "Optical evaluation of the large signal behaviour of piezoelectric disc actuators to increase the precision of micro diaphragm pumps," in *Proc. IEEE ACTUATOR; Int. Conf. Exhib. New Actuator Syst. Appl.*, 2021, pp. 1–4.

[29] M. Richter, "Modellierung und experimentelle charakterisierung von mikrofluidsystemen und deren komponenten," Ph.D. dissertation, Fakultät für Elektrotechnik /Institut für Physik, Universität der Bundeswehr München, München, Germany, 1998.

[30] D. Liang et al., "Novel gravimetric measurement technique for quantitative volume calibration in the sub-microliter range," *Meas. Sci. Technol.*, vol. 24, no. 2, 2013, Art. no. 25301, doi: 10.1088/0957-0233/24/2/025301.

[31] Needle Gauge Chart | Syringe Needle Gauge Chart | Hamilton. Accessed: May 31 2023. [Online]. Available: https://www.hamiltoncompany.com/laboratory-products/needles-knowledge/needle-gauge-chart

[32] M. Aliasgari, N. Maleki-Jirsaraei, and S. Rouhani, "The effect of liquid viscosity on sliding friction coefficient of wet granular materials," *EPJ Web Conf.*, vol. 249, 2021, Art. no. 8003, doi: 10.1051/epjconf/202124908003.

[33] B. P. Bruno, A. R. Fahmy, M. Stürmer, U. Wallrabe, and M. C. Wapler, "Properties of piezoceramic materials in high electric field actuator applications," *Smart Mater. Struct.*, vol. 28, 2018, Art. no. 015029.

[34] A. Bußmann et al., "Microfluidic cell transport with piezoelectric micro diaphragm pumps," *Micromachines*, vol. 12, no. 12, 2021, Art. no. 25420, doi: 10.3390/mi12121459.

[35] The Royal Society of Chemistry, "Flow control using audio tones in resonant microfluidic networks: Towards cell-phone controlled lab-on-a-chip devices," 2016. Accessed: Nov. 9, 2023. [Online]. Available: https://pubs.rsc.org/en/content/articlelanding/2016/lc/c6lc00738d

[36] M. Nafea, A. Nawabjan, and M. S. Mohamed Ali, "A wirelessly-controlled piezoelectric microvalve for regulated drug delivery," *Sensors Actuators A: Phys.*, vol. 279, pp. 191–203, 2018, doi: 10.1016/j.sna.2018.06.020.

[37] Physik Instrumente (PI) GmbH & Co. KG, "Piezoelectric actuators: Components, technologies, operation." Accessed: Nov. 12, 2023. [Online]. Available: https://www.physikinstrumente.com/fileadmin/user_upload/pi_ceramic/files/catalog_CAT/PI_CAT128E_R3_Piezoelectric_Actuators.pdf

[38] H. Asadi Dereshgi, H. Dal, and M. Z. Yildiz, "Piezoelectric micropumps: State of the art review," *Microsystem Technol.*, vol. 27, no. 12, pp. 4127–4155, 2021, doi: 10.1007/s00542-020-05190-0.

[39] L. A. Villarruel Mendoza, N. A. Scilletta, M. G. Bellino, M. F. Desimone, and P. N. Catalano, "Recent advances in micro-electro-mechanical devices for controlled drug release applications," *Front. Bioeng. Biotechnol.*, vol. 8, 2020, Art. no. 827, doi: 10.3389/fbioe.2020.00827.

[40] L. Grünerbel, A. Bußmann, and O. Zett, "Optimization of micropump flow rate by phase dependent coupling: Hochflussoptimierung von mikromembranpumpen durch phasengesteuerte kopplung," in *Proc. Mikro System Technik Kongress*, 2019, pp. 758–761.

[41] T. Peng et al., "A high-flow, self-filling piezoelectric pump driven by hybrid connected multiple chambers with umbrella-shaped valves," *Sensors Actuators B: Chem.*, vol. 301, 2019, Art. no. 126961, doi: 10.1016/j.snb.2019.126961.

[42] Z. Yang, L. Dong, M. Wang, X. Li, X. Liu, and G. Liu, "A miniature piezoelectric pump with high performance," *AIP Adv.*, vol. 12, no. 6, 2022, Art. no. 25320, doi: 10.1063/5.0094633.

[43] A. Pager et al., "User experience for manual injection of 2 mL viscous solutions is enhanced by a new prefillable syringe with a staked 8 mm ultra-thin wall needle," *Expert Opin. Drug Del.*, vol. 17, no. 10, pp. 1485–1498, 2020, doi: 10.1080/17425247.2020.1796630.

[44] A. Pager, "8 MM needle – Improving subcutaneous chronic drug delivery," *ONdrugDelivery Magazine*, Oct. 2019. Accessed: Jun. 2, 2023. [Online]. Available: https://www.ondrugdelivery.com/8-mm-needle-improving-subcutaneous-chronic-drug-delivery/